Behavioral Analysis of Anisotropic Diffusion in Image Processing

Yu-Li You, Wenyuan Xu, Allen Tannenbaum, and Mostafa Kaveh, *Fellow, IEEE*

Abstract— In this paper, we analyze the behavior of the anisotropic diffusion model of Perona and Malik. The main idea is to express the anisotropic diffusion equation as coming from a certain optimization problem, so its behavior can be analyzed based on the shape of the corresponding energy surface. We show that anisotropic diffusion is the steepest descent method for solving an energy minimization problem. It is demonstrated that an anisotropic diffusion is well posed when there exists a unique global minimum for the energy functional and that the ill posedness of a certain anisotropic diffusion is caused by the fact that its energy functional has an infinite number of global minima that are dense in the image space. We give a sufficient condition for an anisotropic diffusion to be well posed and a sufficient and necessary condition for it to be ill posed due to the dense global minima. The mechanism of smoothing and edge enhancement of anisotropic diffusion is illustrated through a particular orthogonal decomposition of the diffusion operator into two parts: one that diffuses tangentially to the edges and therefore acts as an anisotropic smoothing operator, and the other that flows normally to the edges and thus acts as an enhancement operator.

I. INTRODUCTION

THERE has been a great deal of interest in anisotropic diffusion since it was first proposed by Perona and Malik [27] as a useful tool for multiscale description of images, image segmentation, edge detection, and image enhancement. The basic idea behind anisotropic diffusion is to evolve from an original image $u_0(x, y)$, defined in a convex domain $\Omega \subset \mathbf{R} \times \mathbf{R}$, a family of increasingly smooth images $u(x, y, t)$ derived from the solution of the following partial differential equation [27]:

$$\frac{\partial u}{\partial t} = \text{div}\left[c(|\nabla u|)\nabla u\right] \qquad (1)$$

with initial condition $u(x, y, 0) = u_0(x, y)$. The diffusion coefficient $c(\cdot)$ is a nonnegative function of the magnitude of local image gradient $|\nabla u| = \sqrt{u_x^2 + u_y^2}$. The desirable diffusion coefficient should be such that (1) diffuses more in smooth areas and less around large intensity transitions, so that small variations in image intensity such as noise

and unwanted texture are smoothed and edges are preserved. Another objective for the selection of $c(\cdot)$ is to incur backward diffusion around large intensity transitions so that edges are sharpened, and to assure forward diffusion in smooth areas for noise removal. Two such diffusion coefficients suggested by Perona and Malik [28] are

$$c(s) = \exp\left[-\left(\frac{s}{k}\right)^2\right] \qquad (2)$$

and

$$c(s) = \frac{1}{1 + \left(\frac{s}{k}\right)^2} \qquad (3)$$

where k is a constant to be tuned for a particular application.

Unfortunately, it has been widely noted that anisotropic diffusions with diffusion coefficients given by (2) and (3) are ill posed in the sense that images close to each other are likely to diverge during the diffusion process. For example, the presence of noise, especially when the gradient generated by noise is comparable to that by image features, can drive the diffusion process to undesirable results [27], [36]. Even without noise, "staircasing" effects can arise around smooth edges [36]. In practical implementation on computer, the diffusion process may diverge depending on difference schemes and grid sizes [25].

Several arguments about the ill posedness of the anisotropic diffusion are based on the work by Hollig *et al.* [18], which states that one–dimensional (1-D) anisotropic diffusion is well posed if and only if

$$\phi'(s) \geq 0 \qquad (4)$$

where the $\phi(s)$ is a flux function defined as

$$\phi(s) = sc(s). \qquad (5)$$

Since the behavior of two-dimensional (2-D) diffusion is obviously more complex than its 1-D counterpart, a thorough behavioral analysis of 2-D anisotropic diffusion would benefit further development of powerful anisotropic diffusion schemes.

The ill-posedness of anisotropic diffusion may be alleviated through the introduction of a smoothing operation to the variable of diffusion coefficient $c(s)$. One such example [8] is

$$\frac{\partial u}{\partial t} = \text{div}\left\{c[|\nabla G(s) * u|]\nabla u\right\} \qquad (6)$$

where $G(s) * u$ denotes a convolution of the image at time t with a Gaussian kernel of scale s, which is to be given *a priori*.

A properly selected s is critical to the success of the proposed anisotropic diffusion in the sense that the diffusion process would be ill posed for too small an s, while image features would be smeared for too large an s. One possible solution is to use a large s initially to suppress noise and then to reduce the s so that image features are not further smeared [36]. Nevertheless, optimum selection of such an s is still an open problem. The computational load involved in the convolution $G(s) * u$ is a serious problem because it is required at each time instant, whether it is implemented directly or by a separate isotropic diffusion. We also note that this peculiar scheme of linear isotropic diffusion within anisotropic diffusion is obviously against the spirit of anisotropic diffusion. Time-delay regularizations have also been proposed; see [19].

An alternative is to use curve evolution, which is based on geometric heat flow of the level sets of the image. Diffusion schemes proposed include curvature motion [1]–[3], [21], [26], [32], reaction-diffusion [20], and affine invariant scale-space [2], [30].

This paper will express anisotropic diffusion as resulting from an optimization problem. This is in the spirit of the total variational methods of [29]. We show that anisotropic diffusion is an energy-dissipating process, so its behavior can be analyzed by the shape of the energy surface. Specifically, we show in Section II that anisotropic diffusion is a process that dissipates energy with time, and its behavior depends on the shape of the energy surface. Section III gives conditions for the well-posedness and ill-posedness of anisotropic diffusions. Section IV proposes an orthogonal decomposition of the anisotropic diffusion operation and its geometric interpretation, which gives some insights into how anisotropic diffusion smooths small variations in image intensity and sharpens edges. Section V analyzes some known anisotropic diffusion schemes as well as proposes new ones. Section VI outlines our plans of extending to vector case (in particular, the color space). Numerical simulations are shown in Section VII. We conclude this paper in Section VIII.

II. DIFFUSION AS AN ENERGY-DISSIPATING PROCESS

In this section, we demonstrate that anisotropic diffusion results from an optimization problem and relate its behavior to the shape of the corresponding cost (or energy) functional.

A. Smooth Images

Let us first consider the following energy functional defined on the space of smooth images, that is, images for which ∇u is finite in Ω, as in the following:

$$E(u) = \int_\Omega f(|\nabla u|)\, d\Omega \qquad (7)$$

where $f(|\nabla u|) \geq 0$ is an increasing function of $|\nabla u|$, as follows:

$$f'(|\nabla u|) > 0. \qquad (8)$$

We also require that $f'(|\nabla u|) = 0$ when $|\nabla u| = 0$. Due to the nonnegativity of $f(|\nabla u|)$, the energy functional is bounded below:

$$E(u) \geq 0. \qquad (9)$$

Since $|\nabla u| \geq 0$ and $f(|\nabla u|)$ is an increasing function of $|\nabla u|$, the global minimum of $E(u)$ occurs when

$$u(x, y) \equiv \text{constant}, \quad \text{for all} \quad (x, y) \in \Omega. \qquad (10)$$

This global minimum includes an infinite number of constant images, all of which have the same value of $E(u)$. This energy functional is a measure of image smoothness and its minimization is equivalent to smoothing. Note that if $f(x) = x$, (7) is the seminorm of the space of functions of bounded variation and is used as the basis for the total variation-based noise removal algorithm in [29].

We now seek to minimize $E(u)$ by considering the first Gâteaux variation of $E(u)$ at u in the direction h [34], as follows:

$$dE(u; h) = \lim_{\lambda \to 0} \frac{E(u + \lambda h) - E(u)}{\lambda}. \qquad (11)$$

We need to identify conditions under which

$$dE(u; h) = 0 \quad \text{for small} \quad h. \qquad (12)$$

Let $\Omega_0 = \{(x, y) : |\nabla u(x, y)| = 0,\ (x, y) \in \Omega\}$, the Gâteaux variation can be obtained through some elementary calculus as

$$dE(u; h) = f'(0) \int_{\Omega_0} |\nabla h|\, d\Omega$$
$$+ \int_{\Omega - \Omega_0} f'(|\nabla u|) \frac{\nabla u}{|\nabla u|} \cdot \nabla h\, d\Omega. \qquad (13)$$

Let us choose an h such that

$$|\nabla h| \neq 0, \quad (x, y) \in \Omega_0; \qquad (14)$$
$$|\nabla h| = 0, \quad \text{otherwise}. \qquad (15)$$

Then the second term of (13) is zero, but the first term is not. In order for $dE(u; h) = 0$, we must have

$$f'(0) = 0. \qquad (16)$$

We can write the first term of (13) as

$$\int_{\Omega_0} f'(|\nabla u|) \frac{\nabla u}{|\nabla u|} \cdot \nabla h\, d\Omega \qquad (17)$$

if we denote $\vec{0} = [0, 0]^T$ and define

$$\left. \frac{\nabla u}{|\nabla u|} \right|_{\nabla u = \vec{0}} = \vec{0}. \qquad (18)$$

Then the two terms in (13) can be packed together to give

$$dE(u; h) = \int_\Omega f'(|\nabla u|) \frac{\nabla u}{|\nabla u|} \cdot \nabla h\, d\Omega. \qquad (19)$$

By Green's theorem, we have

$$dE(u; h) = -\int_\Omega \text{div}\left[f'(|\nabla u|) \frac{\nabla u}{|\nabla u|} \right] h\, d\Omega$$
$$+ \oint_{\partial \Omega} f'(|\nabla u|) \frac{\nabla u}{|\nabla u|} \cdot \vec{n} h\, d\partial \Omega \qquad (20)$$

where $\partial\Omega$ is the boundary of image domain Ω and $\vec{n}$ is the outward normal to $\partial\Omega$. If we assume symmetric boundary condition for the image

$$\nabla u(x, y) \cdot \vec{n} \equiv 0 \quad \text{for} \quad (x, y) \in \partial\Omega \tag{21}$$

the second term of (20) vanishes and the Gâteaux variation can then be expressed as

$$dE(u; h) = \langle \nabla E(u), h \rangle \tag{22}$$

where $\langle \cdot, \cdot \rangle$ is the inner product defined by

$$\langle f, g \rangle = \int_\Omega f(x, y)g(x, y) \, d\Omega \tag{23}$$

and

$$\nabla E(u) = -\text{div}\left[f'(|\nabla u|)\frac{\nabla u}{|\nabla u|}\right] \tag{24}$$

is the gradient of $E(u)$ at u.

Similar to steepest descent, we may minimize the functional $E(u)$ by moving in the negative direction of the gradient through the following parabolic partial differential equation:

$$\frac{\partial u}{\partial t} = -\nabla E(u)$$
$$= \text{div}\left[f'(|\nabla u|)\frac{\nabla u}{|\nabla u|}\right]. \tag{25}$$

Obviously, (25) is the same as the anisotropic diffusion (1) if the diffusion coefficient is set to

$$c(|\nabla u|) = \frac{f'(|\nabla u|)}{|\nabla u|}. \tag{26}$$

As required of a diffusion coefficient, it is nonnegative due to (8). It is also obvious that the flux function used for 1-D diffusion [see (5)] is

$$\phi(s) = sc(s) = f'(s). \tag{27}$$

Since the energy functional is bounded below [see (9)], the stability of the system given by (25) can be proved by showing that the system dissipates energy with time. The time derivative of the energy functional $E[u(t)]$ of the system is

$$\frac{dE[u(t)]}{dt} = \lim_{\lambda \to 0}\frac{E(u + \lambda h) - E(u)}{\lambda}\bigg|_{h=-\nabla E(u)} \tag{28}$$

which is the Gâteaux variation (11) of $E(u)$ at $u(t)$ in the direction of $h = -\nabla E(u)$. Consequently, we have by (22)

$$\frac{dE[u(t)]}{dt} = \langle \nabla E(u), -\nabla E(u) \rangle$$
$$= -\langle \nabla E(u), \nabla E(u) \rangle$$
$$\leq 0 \tag{29}$$

which indicates that the anisotropic diffusion is indeed an energy-dissipating process with time. Therefore, the anisotropic diffusion is a motion that seeks out minima of $E(u)$ and comes to a stop at stationary points where

$$\nabla E(u) = 0. \tag{30}$$

Since the energy functional is a measure of image smoothness, the energy-dissipating process of anisotropic diffusion
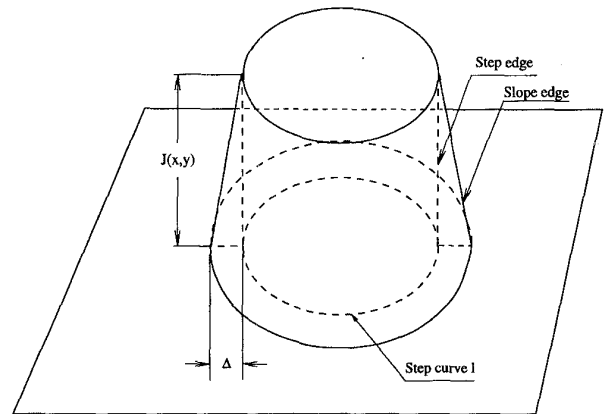

Fig. 1. Interpretation of integral by impulse function when there are step edges in the image.
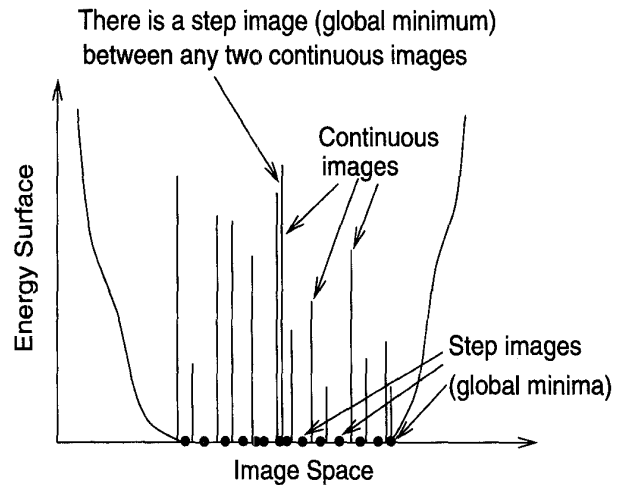

Fig. 2. Illustration of the reason that some anisotropic diffusion models are ill posed.

(25) gives a continuum of images with increasing degrees of smoothness. The behavior of anisotropic diffusion is obviously dependent on the shape of the energy surface. If the global minimum given by (10) is the unique minimum of the energy surface, the diffusion process will converge to it starting from any initial image. The anisotropic diffusion may then be interpreted as "well posed." On the other hand, we will show that, under a certain condition, the energy functional will have an infinite number of global minima, which are dense in the image space, so the anisotropic diffusion is ill posed because the diffusion process, starting from images close to each other, will be caught in different local minima, and we will observe that images close to each other diverge during the diffusion process.

The well posedness, or the argument that the global minimum given by (10) is the unique minimum of the energy surface, is critical to the use of anisotropic diffusion as a tool for scale space filtering. If there exist local minima on the energy surface, the diffusion process may be trapped in one of them and the smoothness of the image will stay at a level
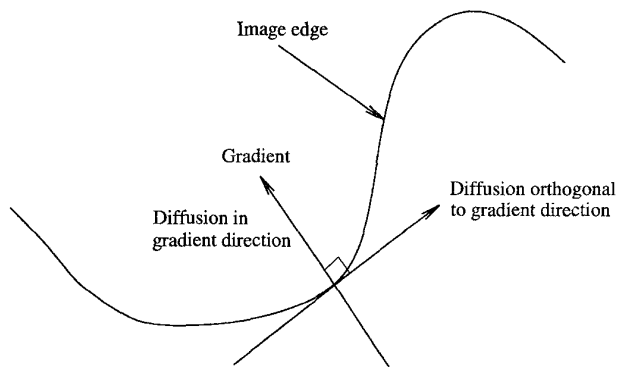
Fig. 3.   Orthogonal decomposition of anisotropic diffusion.

higher than that of the global minima. Correspondingly, the resolution of the image will stay at a level higher than that of the global minimum and *the integration time t is no longer a valid scale-space parameter.*

B. Piecewise Smooth Images

The above derivation has been based on an energy functional $E(u)$ defined on the space of smooth images. Since an interesting image containing edges is better modeled by piecewise smoothness, it is the task of this section to extend the definition of the energy functional $E(u)$ and the general results of last subsection to piecewise smooth images. Let $\mathbf{I}(\Omega)$ denote the image space that is defined to be the set of piecewise smooth functions on Ω with discontinuities being only step edges. The primary difficulty in extending the definition of $E(u)$ to this image space is that the magnitude of gradient $|\nabla u|$ is infinite at step edges. If the integral in (7) is understood in the usual sense, the step edges will not contribute to the value of the energy functional. This is obviously not reasonable in the present context because step edges are rough images in our image space. A strict treatment would involve Lebesgue–Stieltjes integral. But here we forego strict mathematical rigor and resort to the use of the Dirac delta function.

An image $u(x, y) \in \mathbf{I}(\Omega)$ may be written as

$$u(x, y) = w(x, y) + s(x, y) \qquad (31)$$

where the $w(x, y)$ is the smooth part of $u(x, y)$ and $s(x, y)$ represents its step edges, which we call a "step image" and define as follows.

Definition 1—Step Image: Let S be a subset of Ω. The function defined by

$$\chi_s(x, y) = \begin{cases} 1, & (x, y) \in S; \\ 0, & \text{otherwise} \end{cases} \qquad (32)$$

is known as the *characteristic function* of S. A *step image* is a linear combination of a finite number of characteristic functions. Specifically, let Ω_i, $i = 1, 2, \cdots, n$ be a partition of Ω; then the step image is

$$s(x, y) = \sum_{i=1}^{n} s_i \chi_{\Omega_i}(x, y) \qquad (33)$$

where the s_i, $i = 1, 2, \cdots, n$ are constants and are required in this paper not to be equal for adjacent Ω_i's. As an example, we give the following step image:

$$s(x, y) = \begin{cases} s_1, & x_0 \le x < x_1 \\ s_2, & x_1 \le x < x_2 \\ s_3, & x_2 \le x \le x_3 \end{cases} \qquad (34)$$

where $s_1 \ne s_2$ and $s_2 \ne s_3$.

The integral in (7) can then be written as the sum of the following two integrals:

$$E(u) = E(w) + E(s) \qquad (35)$$

where the $E(w)$ involves the usual integral with a smooth integrand and the $E(s)$ is the integral with a step image as its integrand. We discuss the latter integral using impulse functions as follows. Let us suppose that $s(x, y)$ consists of a step edge along a curve l (not necessarily connected nor closed) with a jump of $J(x, y)$ (shown in Fig. 1). We approximate this step edge by a slope edge $v(x, y; \Delta)$ (Fig. 1) with a width of Δ, so the magnitude of the gradient at the slope is

$$|\nabla v(x, y; \Delta)| = \frac{|J(x, y)|}{\Delta}. \qquad (36)$$

This is an impulse function as $\Delta \to 0$, because it tends to ∞ and its area tends to $\Delta \, [|J(x, y)|]/\Delta = |J(x, y)|$. We now integrate $E(v)$ in the direction orthogonal to that of l and then integrate along l. This gives us

$$E(v) = \int_l \Delta f\left[\frac{|J(x, y)|}{\Delta}\right] dl. \qquad (37)$$

Since $v(x, y; \Delta) \to s(x, y)$ as $\Delta \to 0$, we have

$$
\begin{aligned}
E(s) &= \lim_{\Delta \to 0} \int_l \Delta f\left[\frac{|J(x, y)|}{\Delta}\right] dl \\
&= \int_l \lim_{\Delta \to 0} \frac{f\left[\frac{|J(x, y)|}{\Delta}\right]}{\frac{1}{\Delta}} dl \\
&= \begin{cases} 0, & f(\infty) < \infty; \\ f'(\infty) \int_l |J(x, y)| \, dl, & f(\infty) = \infty. \end{cases}
\end{aligned} \qquad (38)
$$

Since it is obvious that $f'(\infty) = 0$ whenever $f(\infty) < \infty$, the above equation can be simplified to give

$$E(s) = f'(\infty) \int_l |J(x, y)| \, dl \qquad (39)$$

which is actually a line integral of the jump of the step edge. This is a generalization of the results in [1].

With the previous extended definition of the energy functional $E(u)$, we can show that the expressions of $dE(u; h)$ (19) and $\nabla E(u)$ (24) are still valid, except that all the derivatives involved are generalized derivatives. Therefore, the relation between anisotropic diffusion and the energy functional discussed in last section can be used to give an analysis about the behavior of anisotropic diffusion.

III. SHAPE OF THE ENERGY SURFACE AND BEHAVIOR OF ANISOTROPIC DIFFUSION

Having the relation between anisotropic diffusion and the energy functional $E(u)$, we can now proceed to analyze the behavior of anisotropic diffusion based on an analysis of the shape of the energy functional. We do this by identifying conditions for the existence of stationary points of $E(u)$ and analyzing the nature of the stationary points.

Definition 2: An image $u \in \mathbf{I}(\Omega)$ is a stationary point of $E(u)$ if

$$dE(u; h) = 0, \quad \text{for all small} \quad h \in \mathbf{I}(\Omega) \tag{40}$$

or equivalently, if

$$\nabla E(u) = 0. \tag{41}$$

A. Ill-Posed Anisotropic Diffusion

We will show in this subsection that, under a certain condition, the energy functional $E(u)$ has an infinite number of global minima (step images) that are dense in the image space. So the diffusion process, starting from images no matter how close to each other, will be caught in different local minima. Consequently, we observe that images close to each other diverge as the diffusion process evolves, so the anisotropic diffusion is ill posed.

Let us consider the step image (33) and denote $\tilde{\Omega} = \bigcup_{i=1,2,\cdots,n} \partial\Omega_i$ where $\partial\Omega_i$ is the boundary of Ω_i, respectively. Then the gradient of the image (33) can easily be obtained as

$$|\nabla u(x, y)| = \begin{cases} \infty, & (x, y) \in \tilde{\Omega} \\ 0, & \text{otherwise.} \end{cases} \tag{42}$$

For the example image (34), this is

$$|\nabla u(x, y)| = (s_2 - s_1)\delta(x - x_1) + (s_3 - s_2)\delta(x - x_2) \tag{43}$$

where $\delta(x)$ is the Dirac impulse function.

Theorem 1: Each of the step images (33), which are dense in the image space $\mathbf{I}(\Omega)$, is a stationary point of $E(u)$ if and only if

$$f'(\infty) = 0. \tag{44}$$

Proof: Let us first note that step images are dense in the image space $\mathbf{I}(\Omega)$ because each continuous signal can be infinitely approximated by a sequence of step signals; that is, for each continuous signal u there exists a sequence of step signals $\{s_n\}$, $n = 1, 2, \cdots$ such that

$$\lim_{n \to \infty} s_n = u. \tag{45}$$

Let us now prove the "if" part. Since

$$\begin{aligned} 0 &\le \lim_{|\nabla u| \to \infty} \left| f'(|\nabla u|) \frac{\nabla u}{|\nabla u|} \right| \\ &= \lim_{|\nabla u| \to \infty} f'(|\nabla u|) \left| \frac{\nabla u}{|\nabla u|} \right| \\ &= f'(\infty) = 0 \end{aligned} \tag{46}$$

we have

$$f'(|\nabla u|) \frac{\nabla u}{|\nabla u|} = 0, \quad \text{for} \quad (x, y) \in \tilde{\Omega}. \tag{47}$$

Due to (16) and (18), we have

$$f'(|\nabla u|) \frac{\nabla u}{|\nabla u|} = 0, \quad \text{for} \quad (x, y) \in \Omega - \tilde{\Omega}. \tag{48}$$

Combining (47) and (48) we have

$$f'(|\nabla u|) \frac{\nabla u}{|\nabla u|} \equiv 0, \quad \text{for} \quad (x, y) \in \Omega \tag{49}$$

which indicates $\nabla E(u) \equiv 0$ by (24).

Let us now prove the "only if" part. Consider the Gâteaux variation (19) of $E(u)$ at the step image s in the direction $h = s$, as follows:

$$dE(s; s) = \int_\Omega f'(|\nabla s|)|\nabla s|\, d\Omega. \tag{50}$$

Since $f'(|\nabla s|)|\nabla s| = 0 = f'(\infty)|\nabla s|$ when $|\nabla s| = 0$, the last equation can be written as

$$dE(s; s) = \int_\Omega f'(\infty)|\nabla s|\, d\Omega \tag{51}$$

which, when interpreted by (39), is

$$dE(s; s) = f'(\infty) \int_l |J(x, y)|\, dl. \tag{52}$$

For the step image (33), the integral in the last equation is not zero, so $dE(s; s) = 0$ only if $f'(\infty) \ne 0$. This completes the proof. ∎

The following theorem illustrates the nature of the stationary points.

Theorem 2: If the $f(\cdot)$ of an anisotropic diffusion satisfies (44), then each of the dense step images (33) is a global minimum of $E(u)$ and the $E(u)$ is discontinuous for all smooth images except for the constant image (10).

Proof: For a step image s, the w in (31) is a constant image, and we find from (39) that $E(s) = 0$ due to (33), so (35) gives

$$E(s) = E(\text{constant image}) \tag{53}$$

which is the same value as that of the global minimum (10) of $E(u)$. So each of the step images (33) is a global minimum of $E(u)$.

Let us consider (45), which states that a continuous signal u can always be infinitely approximated by a sequence of step signals s_n, $n = 1, 2, \cdots$. For a continuous image u, it is obvious that $E(u) \ne 0$ except that u is the constant image (10). On the other hand, the conditions (39) and (44) give $E(s_n) = 0$, $n = 1, 2, \cdots$, so that

$$\lim_{n \to \infty} E(s_n) = 0 \ne E(u). \tag{54}$$

Therefore, $E(u)$ is not continuous at u except for the constant image (10). ∎

We now give a simplified illustration of how anisotropic diffusion is ill posed (see Fig. 2). We compare our image space to the real line, continuous images to rational numbers,
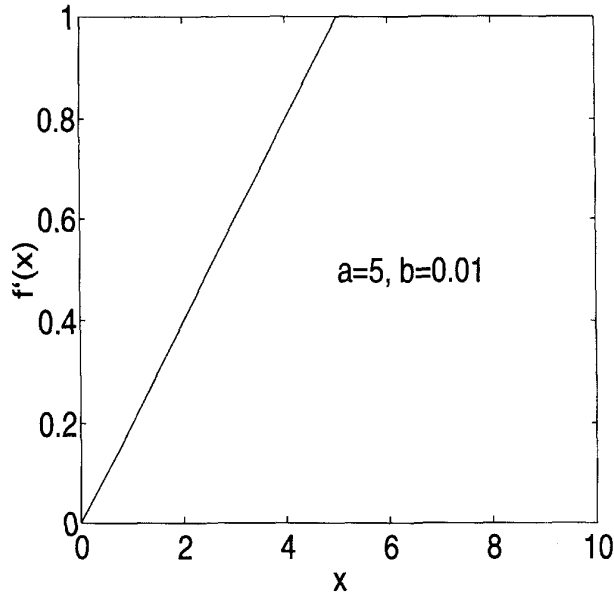
Fig. 4. Example of modified $f'(\cdot)$.

and step images to irrational numbers. Then, according to Theorems 1 and 2, the energy functional has nonzero values for all "rational numbers" and zero values for all "irrational numbers." Since irrational numbers are dense on the real line (there is an irrational number between any two rational numbers), the energy functional is very "rough" and it is not possible to know which one of the dense "irrational numbers" the anisotropic diffusion will settle down to.

B. Well-Posed Anisotropic Diffusion

It is obvious that an anisotropic diffusion is well posed if the constant image given by (10) is the unique global minimum of the energy functional $E(u)$, because the diffusion process, starting from different images, will get closer and closer as the diffusion descends toward the global minimum. It is the task of this section to identify conditions for the existence of a unique global minimum.

By Theorem 1 we know that the step image (33) are not a stationary point of $E(u)$ if $f'(\infty) \neq 0$. This result is now extended to give the following theorem.

Theorem 3: Only the constant image (10) is the stationary point of $E(u)$ if

$$f'(\infty) \neq 0. \tag{55}$$

Proof: Theorem 1 has shown that step images (33) are not a stationary point of $E(u)$; we need only to show that smooth images are not either. Consider the Gâteaux variation (19) of $E(u)$ at a smooth image u in the direction $h = u$, as follows:

$$dE(u;\, u) = \int_\Omega f'(|\nabla u|)|\nabla u|\, d\Omega. \tag{56}$$

Let us assume that the smooth image u is not a constant image, then there exists at least some area $\Omega' \subset \Omega$ in which $|\nabla u| \neq 0$.

Then the integrand is positive in this area due to (8); hence, it is not possible that the integral is zero for a smooth image, except for the constant image (10). Therefore, all images in $\mathbf{I}(\Omega)$, except for the constant image (10), are not the stationary point of $E(u)$. ∎

This theorem basically establishes that, if (55) holds, the constant image (10) is the unique global minimum of $E(u)$. But this does not exclude the possibility that the surface of $E(u)$ is still irregular in the sense that the diffusion process may still exhibit some strange behavior even though it will finally converge to the constant image (10). For example, the diffusion given by (92) has $f'(\infty) = 1 \neq 0$, so the constant image is the unique global minimum by the last theorem. But a step-image-like effect still appears during the diffusion process (see the right of Fig. 5 and the bottom of Fig. 6) though it finally disappears, as required by the last theorem. Therefore, we need conditions stronger than (55) to make the surface of $E(u)$ regular enough to prevent the step-image-like effect to appear during the diffusion process. One way to achieve this is to require that $E(u)$ be convex.

Theorem 4: If the $f(\cdot)$ of an anisotropic diffusion is convex, then its energy functional $E(u)$ is convex and the constant image (10) is its unique global minimum.

Proof: Let $u_1,\, u_2 \in \mathbf{I}(\Omega)$ with $u_1 \neq u_2$; then, for each $\lambda \in (0,\, 1)$, we have the following by the Minkowski inequality [24]:

$$|\nabla[\lambda u_1 + (1 - \lambda)u_2]| \leq \lambda|\nabla u_1| + (1 - \lambda)|\nabla u_2|. \tag{57}$$

Since $f(\cdot)$ is strictly increasing (refer to (8)), (57) gives

$$f\{|\nabla[\lambda u_1 + (1 - \lambda)u_2]|\} \leq f[\lambda|\nabla u_1| + (1 - \lambda)|\nabla u_2|]. \tag{58}$$

The convexity of $f(\cdot)$ gives

$$f[\lambda|\nabla u_1| + (1 - \lambda)|\nabla u_2|] \leq \lambda f(|\nabla u_1|) + (1 - \lambda)f(|\nabla u_2|). \tag{59}$$

Combining (58) and (59), we have

$$f\{|\nabla[\lambda u_1 + (1 - \lambda)u_2]|\} \leq \lambda f(|\nabla u_1|) + (1 - \lambda)f(|\nabla u_2|). \tag{60}$$

Integrating (60) gives

$$\int_\Omega |\nabla[\lambda u_1 + (1 - \lambda)u_2]|\, d\Omega \leq$$
$$\lambda \int_\Omega f(|\nabla u_1|)\, d\Omega + (1 - \lambda) \int_\Omega f(|\nabla u_2|)\, d\Omega \tag{61}$$

which is

$$E[\lambda u_1 + (1 - \lambda)u_2] \leq \lambda E(u_1) + (1 - \lambda)E(u_2). \tag{62}$$

Therefore, the functional $E(u)$ is convex.

Now we prove the second half of the theorem using Theorem 3 and the fact that $f'(\infty) \neq 0$ if $f(\cdot)$ is convex. Let us first note a theorem in [6], which states that the $f(\cdot)$ is convex if and only if

$$f(x) \geq f(x_0) + f'(x_0)(x - x_0) \quad \text{for all} \quad x_0, x \geq 0. \tag{63}$$

If we let $x_0 = \infty$ and assume that $f'(x_0) = f'(\infty) = 0$, the above inequality gives

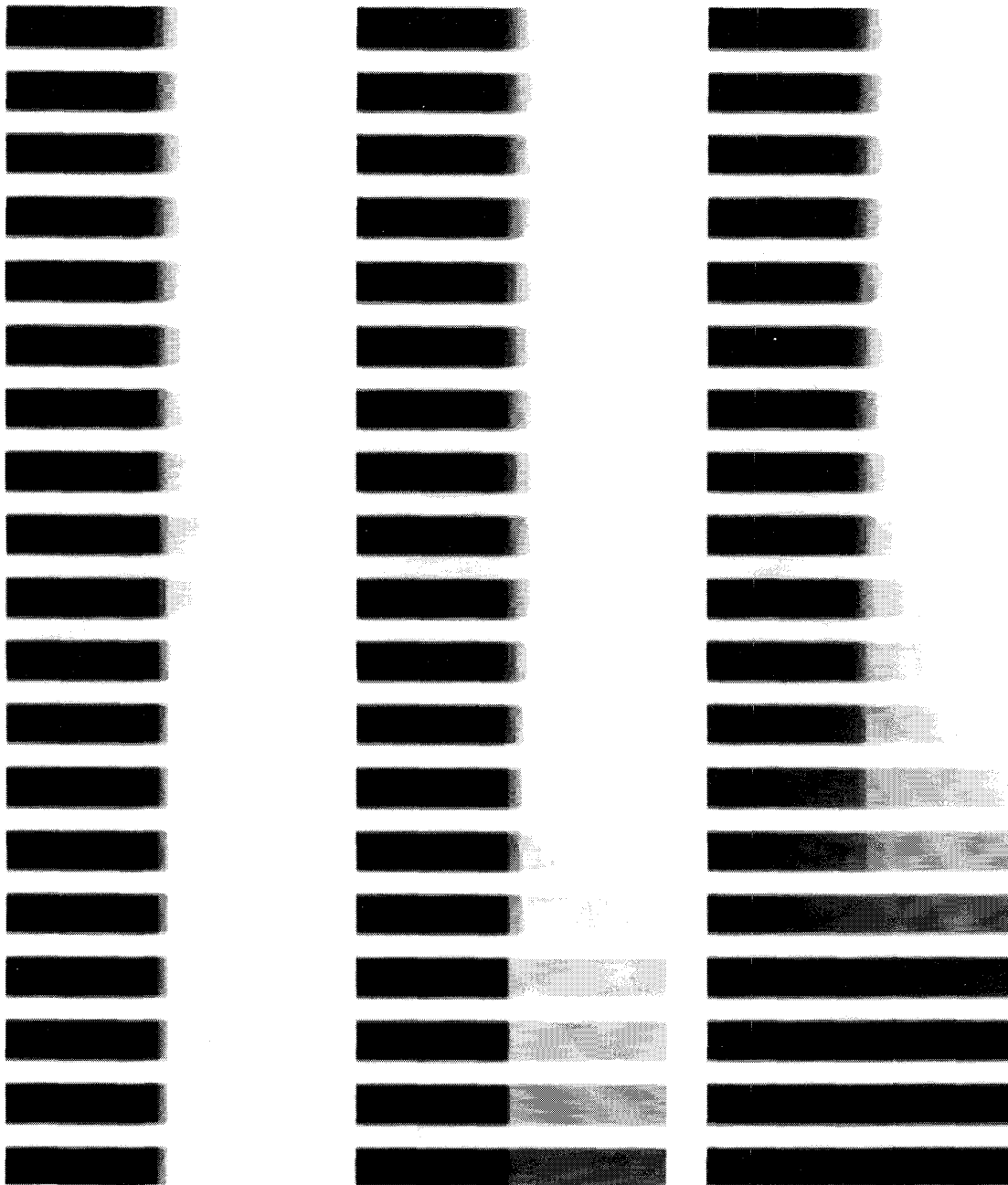$$f(x) \geq f(\infty) \quad \text{for all} \quad x \geq 0 \tag{64}$$

Fig. 5. Smooth sigmoid image is changed into step images by anisotropic diffusion. From top to bottom, the diffusion time $t = 2^n$, $n = 0, 1, \cdots, 18$. Left column: Perona and Malik's diffusion. Middle column: extended version of the diffusion scheme previously developed by the authors. Right column: diffusion scheme that does not have step images as its stationary points, though step images appeared anyway.

which contradicts with the fact that $f(\cdot)$ is increasing. Therefore, we must have $f'(\infty) \neq 0$, and by Theorem 3 we complete the proof. ∎

Step edges are accounted for in the above proof because the proof does not use any properties related to the interpretation problem of the integral. Actually, we can verify in the following that the above theorem does hold for step images. Suppose s_1, $s_2 \in \mathbf{I}(\Omega)$ with $s_1 \neq s_2$ are two step images with their step edges along the curves l_1 and l_2. Let $l = l_1 \bigcup l_2$ and J_1

and J_2 be the jumps of s_1 and s_2, respectively. Then by (39) and the Minkowski inequality [24], we have

$$E[\lambda s_1 + (1 - \lambda)s_2]$$
$$= f'(\infty) \int_l |\lambda J_1 + (1 - \lambda)J_2| \, dl$$
$$\leq \lambda f'(\infty) \int_l |J_1| \, dl + (1 - \lambda)f'(\infty) \int_l |J_2| \, dl$$
$$= \lambda E(s_1) + (1 - \lambda)E(s_2) \tag{65}$$

which is the same as what (62) would give for step edges when its integral is interpreted by (39).

Corollary 1: If $f''(x) \geq 0$ for all $x \geq 0$, then the constant image (10) is the unique global minimum of $E(u)$ and the anisotropic diffusion is well posed.

Proof: This is obvious by a theorem in [6], which states that $f(\cdot)$ is convex if and only if $f''(x) \geq 0$ for all $x \geq 0$. ∎

Remark 1: Another proof is given in [37].

IV. AN ORTHOGONAL DECOMPOSITION AND ITS GEOMETRIC INTERPRETATION

After having discussed the global behavior of anisotropic diffusion, we would like to give some insights into how anisotropic diffusion works locally to enhance or smear edges, or to smooth or magnify noise.

A. An Orthogonal Decomposition

At a specific location $(x, y) \in \Omega$, the behavior of anisotropic diffusion (25) is obviously dependent on $f'[|\nabla u(x, y)|]$ which, in turn, depends on the characteristics of $f[|\nabla u(x, y)|]$. For optimization purposes, which is the case at hand, $f[|\nabla u(x, y)|]$ is best characterized by the eigenstructure of its Hessian matrix

$$H(x, y) = \begin{bmatrix} \dfrac{\partial^2 f(|\nabla u|)}{\partial x^2} & \dfrac{\partial^2 f(|\nabla u|)}{\partial x \, \partial y} \\ \dfrac{\partial^2 f(|\nabla u|)}{\partial y \, \partial x} & \dfrac{\partial^2 f(|\nabla u|)}{\partial y^2} \end{bmatrix}. \quad (66)$$

The eigenvalues of the $H(x, y)$ can be shown to be

$$\lambda_1(|\nabla u|) = \frac{f'(|\nabla u|)}{|\nabla u|}$$

and

$$\lambda_2(|\nabla u|) = f''(|\nabla u|). \quad (67)$$

By (26), it is obvious that $\lambda_1(|\nabla u|) = c(|\nabla u|)$. The anisotropic diffusion (25) can then be expanded into

$$\frac{\partial u}{\partial t} = \lambda_1 D_o + \lambda_2 D_g \quad (68)$$

where

$$D_o = \frac{u_x^2 u_{yy} - 2u_x u_y u_{xy} + u_y^2 u_{xx}}{u_x^2 + u_y^2} \quad (69)$$

and

$$D_g = \frac{u_x^2 u_{xx} + 2u_x u_y u_{xy} + u_y^2 u_{yy}}{u_x^2 + u_y^2} \quad (70)$$

are the second-order directional derivatives of u in directions orthogonal and parallel to the local gradient, respectively. Since the two second-order directional derivatives are in orthogonal directions, (68) represents an orthogonal decomposition of anisotropic diffusion (see Fig. 3). We note here that the idea of degenerate diffusion was previously mentioned in [1].

Since the diffusion coefficient is nonnegative due to (8), the first term of (68) represents a degenerate forward diffusion in the direction orthogonal to the gradient. Thus, this directional smoothing should be encouraged since it represents a well
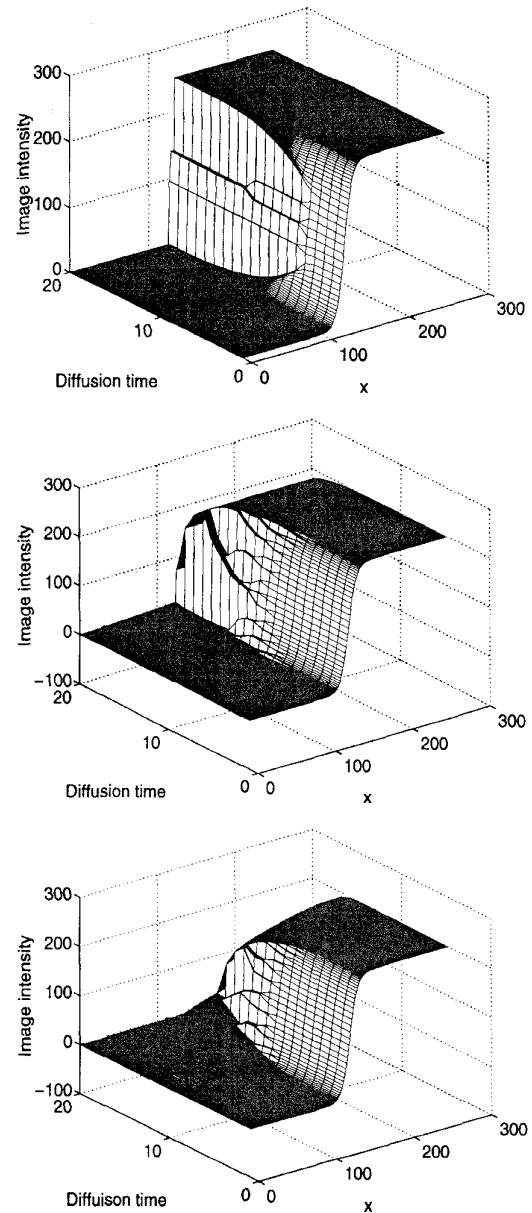

Fig. 6. Evolution with time of a slice along the x axis of the smooth sigmoid image when it is processed by anisotropic diffusion. Note that the indexes in the "Diffusion time" axis are the powers of 2. Top: Perona and Malik's diffusion. Middle: extended version of the diffusion scheme previously developed by the authors. Bottom: diffusion scheme that does not have step images as its stationary points, though step images appeared anyway.

posed smoothing operator that tends to preserve edges, since an edge is also orthogonal to the gradient.

The second term of (68) represents a degenerate diffusion in the direction of the local gradient. It is forward (smoothing) if $\lambda_2(|\nabla u|) > 0$, and backward (sharpening) if $\lambda_2(|\nabla u|) < 0$. Since backward diffusion may be ill posed, there exist possibilities that the whole system of (68) is ill posed if $\lambda_2(|\nabla u|) < 0$ for some $|\nabla u| \geq 0$. This depends on the balance between the forces represented by the first term of (68) and the

Fig. 7. Top: Original Lena image. Bottom: Degraded by 10-dB Gaussian noise.

second term (where $\lambda_2(|\nabla u|) < 0$). If the force represented by the first term dominates for all $|\nabla u| \geq 0$, the system is well posed. Otherwise, the system is ill posed and images close to each other may diverge during the diffusion process.

B. Geometric Interpretation

Let us now give several geometric insights into the decomposition (68). We will only outline the mathematical details here referring the reader to [11] for a complete treatment.

First of all, we write (68) in the following form:

$$\frac{\partial u}{\partial t} = \lambda_1 \kappa |\nabla u| + \lambda_2 \kappa_\perp |\nabla u| \tag{71}$$

where

$$\kappa = \frac{u_x^2 u_{yy} - 2u_x u_y u_{xy} + u_y^2 u_{xx}}{(u_x^2 + u_y^2)^{3/2}} \; \operatorname{div}\left(\frac{\nabla u}{|\nabla u|}\right) \tag{72}$$

and

$$\kappa_\perp = \frac{u_x^2 u_{xx} + 2u_x u_y u_{xy} + u_y^2 u_{yy}}{(u_x^2 + u_y^2)^{3/2}}. \tag{73}$$

Fig. 8. Images processed by Perona and Malik's anisotropic diffusion. Top: $t = 16$. Middle: $t = 128$. Bottom: $t = 4096$.

Note that κ is precisely the mean curvature of the level sets of the function $u(x, y)$ [1], [12]. In fact, the evolution equation

$$\frac{\partial u}{\partial t} = \kappa |\nabla u| \tag{74}$$

is the level set evolution version of Euclidean curve shortening in the plane that has been the object of much study recently

Fig. 9. Performance comparison of Rudin's total variation-based diffusion (top, $t = 25$), its modified version (middle, $t = 25$), and a new scheme (bottom, $t = 50$).

in mathematics and computer vision [1], [14]–[16], [20], [21], [26], [32], [33].

The equation

$$\frac{\partial u}{\partial t} = \kappa_{\perp} |\nabla u| \tag{75}$$

also has a very natural interpretation, and in fact in a very precise sense may be considered to be the dual to (74). In order to make this point precise, we now recall the discussion in the elegant paper of Evans [11].

Accordingly, we consider the following boundary-value problem for the p-Laplacian:

$$\operatorname{div}\left(|\nabla u_p|^{p-2}\nabla u_p\right) = 0 \quad \text{in} \quad \Omega, \tag{76}$$

$$u_p = g \quad \text{on} \quad \partial\Omega \tag{77}$$

when $2 < p < \infty$. This is the Euler–Lagrange equation for the variational problem of minimizing the energy

$$\int_{\Omega} (u_x^2 + u_y^2)^p \, dx \, dy$$

over all sufficiently smooth functions obeying the given boundary condition. (For the exact class of functions, see [11].) Now assuming u_p is smooth and $|\nabla u_p| \neq 0$, we may rewrite (76) to read

$$\frac{1}{(p-2)} \Delta u_p + D_g = 0. \tag{78}$$

Suppose we knew also that as $p \to \infty$, the functions u_p converge in some sufficiently strong sense to a limit u. Then, formally passing to limits in (78), we would expect u to solve the partial differential equation

$$D_g = \kappa_{\perp} |\nabla u| = 0. \tag{79}$$

Accordingly, we define the ∞-Laplacian to be

$$\Delta_{\infty} u = D_g$$
$$= \kappa_{\perp} |\nabla u|.$$

Hence

$$\Delta_{\infty} u = 0 \tag{80}$$

becomes a Euler–Lagrange type equation for an L^{∞}-norm type "energy" minimization problem in the above sense. Given the dual of L^1 is L^{∞} (under certain technical conditions) [28], the dual operator of Δ_{∞} should be derived from the L^1 version of (76), which is precisely

$$\Delta_1 u := \kappa |\nabla u| = \operatorname{div}\left(\frac{\nabla u}{|\nabla u|}\right) |\nabla u| = 0. \tag{81}$$

Note that (80) and (81) are the steady-state versions of (74) and (75). Thus, these arise from dual optimization problems.

Evans [11] notes that in general the equation $\Delta_{\infty} u = 0$ does not admit smooth solutions. Moreover, note that the operator Δ_1 is degenerate, but only in the one direction normal to each level set. On the other hand, the operator Δ_{∞} is nondegenerate only in this direction. As we have seen, $\Delta_1 u = 0$ is a "geometric" equation, since it says that the level sets of u have zero-mean curvature. Thus, the partial differential equation $\Delta_{\infty} u = 0$ is strongly "nongeometric" or, rather, that all its geometric information concerns not the level sets of u but rather the curves normal to level sets. All of this is made precise in the elegant paper of Evans [11].
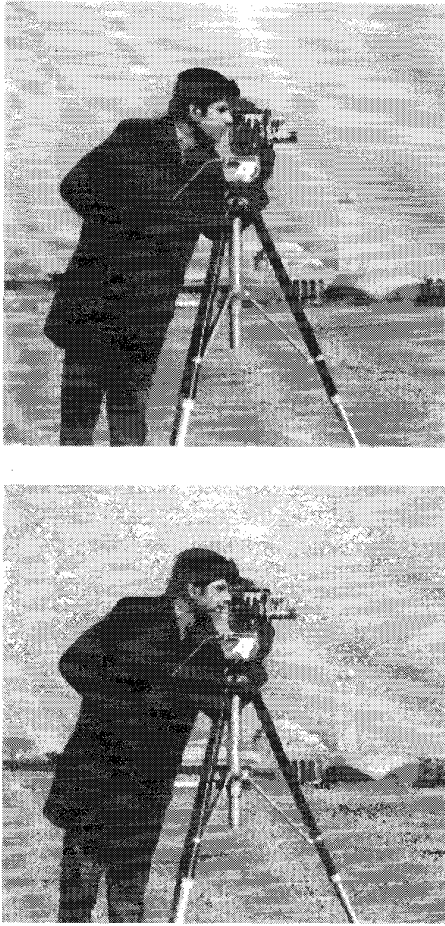
Fig. 10. Top: Original Cameraman image. Bottom: Degraded by 10-dB Gaussian noise.

V. EXAMPLES OF ILL-POSED AND WELL-POSED ANISOTROPIC DIFFUSION

It is easy to show that the $f'(\cdot)$'s for the two diffusion coefficients (2) and (3) are

$$f'(s) = s \, \exp\left[-\left(\frac{s}{k}\right)^2\right] \tag{82}$$

and

$$f'(s) = \frac{s}{1 + \left(\frac{s}{k}\right)^2} \tag{83}$$

respectively, and both of them satisfy the condition (44), so both of them are ill posed. The step images (33) seem to confirm the staircasing effects observed in [36]. The orthogonal decomposition of anisotropic diffusion described in Section IV provides an insight into the smoothing and edge enhancing property of the two anisotropic diffusion schemes as described in [27]: The $f''(\cdot)$'s of the two diffusion schemes have the following thresholding property:

$$f''(x)\begin{cases} \geq 0, & x \leq T \\ < 0, & x > T \end{cases} \tag{84}$$

Fig. 11. Top and middle: Cameraman image processed by Perona and Malik's anisotropic diffusion ($t = 64$ and 2048, respectively). Bottom: Cameraman image processed by a proposed scheme ($t = 64$).

which, according to (68) and Fig. 3, indicates that the two diffusion schemes smooth the image where the image gradient is small and enhance it where the image gradient is large.

The line of research on noise removal based on bounded variation can also be placed into the category of anisotropic diffusion. The original algorithm considers the following constrained minimization problem [29]:

$$\min_u \int_\Omega |\nabla u| \, d\Omega \tag{85}$$

subject to

$$|u - u_0| = \sigma^2 \tag{86}$$

where u_0 is the observed image and σ^2 is the power of observation noise. If we ignore the constraint, (85) is exactly the energy functional $E(u)$ with a $f(x) = x$. The corresponding diffusion coefficient is

$$c(x) = \frac{1}{x}. \tag{87}$$

It is easy to check that $f'(x) = 1$ and $f''(x) = 0$, so this diffusion is well posed by the corollary to Theorem 4. Since $f''(x) \equiv 0$, this diffusion scheme smooths an image only in the direction orthogonal to the gradient, hence it tends not to disturb edges. Note that the fact that $f'(x) = 1$ contradicts the necessary condition (16) was not considered in [29]. However, this problem can be readily bypassed in practical implementation by including the condition of "no diffusion when $|\nabla u| = 0$," which, in effect, forces the condition $f'(0) = 0$ on the algorithm.

The above total variation-based algorithm tends to produce "blocky effects" in smooth areas. This may be attributed to the discontinuity of $f'(x)$ at $x = 0$ and to the oversmoothing in smooth areas because the diffusion coefficient $c(x)$ of (87) is very large when x is very small. In order to treat this problem, we modify the $c(\cdot)$ to

$$c(x) = \begin{cases} \dfrac{1}{T}, & x < T, \\ \dfrac{1}{x}, & x \geq T \end{cases} \tag{88}$$

where T is a parameter to be selected for a particular application. Such an $f(\cdot)$ incurs uniform diffusion wherever the image gradient is small to effectively smooth out noise, while keeping the edge-preserving property of the total variation-based algorithm. Note that the second-order derivative $f''(x)$ of such a $c(\cdot)$ is not continuous at $x = T$. This problem may be dealt with by using the following:

$$f'(x) = \frac{\sqrt{x^2 + b^2} - \sqrt{(x-a)^2 + b^2} - b + \sqrt{a^2 + b^2}}{2a} \tag{89}$$

where a controls the range that $f'(x) \approx x$ and b controls the smoothness of the transition between $f'(x) \approx x$ and $f'(x) \approx 1$. An example of such a $f(\cdot)$ is shown in Fig. 4. Of course, the remedies suggested above do not provide a complete solution to the problem of $|\nabla u|$ vanishing, and further research will be needed to fully resolve the problem.

An extension of the total variation-based diffusion has been proposed in [37], which can be further generalized to give a

$$f(x) = (x + \epsilon)^p, \quad \epsilon > 0 \quad \text{and} \quad 0 < p < 1. \tag{90}$$

Since $f''(x) = p(p-1)(x+\epsilon)^{p-2} < 0$ for $0 < p < 1$, this diffusion scheme has backward diffusion to enhance edges. Unfortunately, this diffusion scheme is ill posed because it satisfies (44), as follows: $f'(\infty) = \lim_{x \to \infty} p(x+\epsilon)^{p-1} = 0$ for $0 < p < 1$. Consequently, it should suffer from problems associated with step images. Indeed, our simulation shows that all input images are transformed into step images with many false step edges. But what is interesting is that all the false step edges gradually disappear as the diffusion proceeds, so that fairly good performance has been observed in [37]. This may be due to the discretization of the problem in digital representation and processing.

This diffusion scheme also tends to produce "blocky effects" in smooth areas because $\lim_{x \to 0} f'(x) = p\epsilon^{p-1} \neq 0$ and we have to redefine $f'(0) = 0$ as required by (16). This can be relieved by modifying the diffusion coefficient $c(\cdot)$ into

$$c(x) = \begin{cases} \dfrac{p(T+\epsilon)^{p-1}}{T}, & x < T \\ \dfrac{p(x+\epsilon)^{p-1}}{x}, & x \geq T \end{cases} \tag{91}$$

which basically incurs uniform diffusion to avoid the "blocky effects."

Finally, we give an example that has backward diffusion and does not satisfy the condition for step images

$$c(x) = \begin{cases} \dfrac{1}{T} + \dfrac{p(T+\epsilon)^{p-1}}{T}, & x < T \\ \dfrac{1}{x} + \dfrac{p(x+\epsilon)^{p-1}}{x}, & x \geq T \\ \epsilon > 0 \quad \text{and} \quad 0 < p < 1. \end{cases} \tag{92}$$

It can be verified that its $f''(x) = p(p-1)(x+\epsilon)^{p-2} < 0$ for $0 < p < 1$ and $x \geq T$, so it has backward diffusion to enhance edges. It can also be verified that $f'(\infty) = 1$, so step images are not its stationary points, according to Theorem 1. Our simulation shows that staircasing effects still appear and then disappear during the diffusion process, with the eventual disappearance satisfying the requirement of Theorem 3.

VI. Vector-Valued Anisotropic Diffusion

The analysis given above basically can be extended for vector-valued anisotropic diffusions, e.g., in color space. This we plan to do in a future publication in which we will discuss such diffusions in detail. In this paper, following Whitaker–Gerig [35], we just want to indicate how anisotropic diffusions may be extended in this framework.

Let $u_0 : \Omega \to D$ be a vector-valued image where $\Omega \subset \mathbf{R}^n$ and $D \subset \mathbf{R}^m$ are open subsets. Then the vector-valued anisotropic evolution equation has the form

$$\frac{\partial u}{\partial t} = \text{div}\,(c\nabla u) \tag{93}$$

where

$$u(x, t) = [u_1(x, t), \cdots, u_m(x, t)]^T$$
$$x = (x_1, \cdots, x_n)^T \in \Omega \tag{94}$$

$$\nabla u = \begin{bmatrix} \dfrac{\partial u_1}{\partial x_1} & \cdots & \dfrac{\partial u_m}{\partial x_1} \\ \vdots & \vdots & \vdots \\ \dfrac{\partial u_1}{\partial x_n} & \cdots & \dfrac{\partial u_m}{\partial x_n} \end{bmatrix} \tag{95}$$

and

$$\text{div}\,(c\nabla u) = \left(\frac{\partial}{\partial x_1}, \cdots, \frac{\partial}{\partial x_n} \right) \cdot c\nabla u. \tag{96}$$

Of course, the key in making this type of diffusion interesting is the choice of the diffusion coefficient c. We can, of course, define independent diffusions in each channel, but a much more interesting choice would be some sort of coupling (this is called a *dissimilarity operator* in [35]) in order to combine the information from the channels. A natural nontrivial choice is

$$|\nabla u|_d := \left[\sum_{i,j}\left(\frac{\partial u_i}{\partial x_j}\right)^2\right]^{1/2}.$$

That is, we take the diffusion coefficient to be of the form

$$c = c(|\nabla u|_d).$$

This operator is a straightforward generalization of the gray-level image case ($m = 1$) and is also rotationally invariant. One may, of course, also smooth the u_i's via a Gaussian filter as in (6).

We plan to apply our eigenvalue analysis to this multidimensional case in a forthcoming paper as well as explicitly apply the results to diffusions in color space.

VII. NUMERICAL SIMULATIONS

We now use numerical simulations to verify the theory just developed and to illustrate some good anisotropic diffusion schemes. The numerical techniques are based on hyperbolic conservation laws and the theory of viscosity solutions [26], [29], [33]. We follow [29] and discretize the anisotropic diffusion (1) in the following manner:

$$u_{ij}^{n+1} =$$
$$u_{ij}^n + \frac{\Delta t}{h}$$
$$\cdot \left(\Delta_-^x\left\{c\left[\sqrt{(\Delta_+^x u_{ij}^n)^2 + m^2(\Delta_+^y u_{ij}^n, \Delta_-^y u_{ij}^n)}\right]\Delta_+^x u_{ij}^n\right\}\right.$$
$$\left.+\Delta_-^y\left\{c\left[\sqrt{(\Delta_+^y u_{ij}^n)^2 + m^2(\Delta_+^x u_{ij}^n, \Delta_-^x u_{ij}^n)}\right]\Delta_+^y u_{ij}^n\right\}\right)$$
$$\tag{97}$$

where Δt and h are the time step size and space grid size, respectively, and

$$\Delta_+^x a_{ij} = a_{i+1,j} - a_{i,j} \tag{98}$$
$$\Delta_-^x a_{ij} = a_{i,j} - a_{i-1,j} \tag{99}$$
$$\Delta_+^y a_{ij} = a_{i,j+1} - a_{i,j} \tag{100}$$
$$\Delta_-^y a_{ij} = a_{i,j} - a_{i,j-1} \tag{101}$$

$$m(a, b) = \begin{cases} \min(a, b), & a > 0 \text{ and } b > 0, \\ \max(a, b), & a < 0 \text{ and } b < 0, \\ 0, & \text{otherwise.} \end{cases} \tag{102}$$

A. Synthesized Image

Let us consider the following smooth sigmoid image:

$$u(x, y) = \frac{255}{1 + \exp\left[-0.2(x - 128)\right]}, \quad x, y = 1, 2, \cdots, 256. \tag{103}$$

We first use Perona and Malik's anisotropic diffusion scheme (2) with $k^2 = 100$ to process this image. The left column of Fig. 5 are the images generated by the anisotropic diffusion at time $t = 2^n$, $n = 0, 1, \cdots, 18$. For each time t, a slice along the x axis of the corresponding image is shown at the top of Fig. 6. Since this diffusion scheme is ill-posed, step images are developed and it does not disappear once it is fully developed.

Next, we run on the same sigmoid image the extended version of the diffusion scheme developed by the authors in [37] whose diffusion coefficient is given by (90) with $p = 0.5$ and $\epsilon = 1$. The corresponding results are shown in the middle column of Fig. 5 and at the middle of Fig. 6. Since this diffusion scheme is also ill posed, step images are developed. But it is interesting that the step images gradually disappear so that the smooth sigmoid edge is transformed into a step edge and the step edge remains over many iterations.

Finally, we run the diffusion scheme given by (92) with $p = 0.5$, $\epsilon = 1$, and $T = 0$, and show the results in the right column of Fig. 5 and at the bottom of Fig. 6. It is evident that staircasing effects appear during the diffusion process, but they disappear because step images are not its stationary points, according to Theorem 1. The difference of this one from the above two diffusion schemes is that the step images appear later and disappear faster. This behavior has been observed on many images.

B. Natural Images

We consider two numerical experiments. In the first experiment, the Lena image shown in Fig. 7 (top) is degraded to give the image shown in Fig. 7 (bottom) using Gaussian noise at a SNR = 10 dB, where

$$\text{SNR} = \frac{\text{Variance of image}}{\text{Variance of noise}}. \tag{104}$$

We first use Perona and Malik's diffusion (2) to process this degraded image and show the results in Fig. 8, which clearly indicate that this diffusion scheme is incapable of dealing with noise. We then compare the performances of Rudin's total variation-based diffusion (87), its modified version (88) with $T = 3$, and the new scheme given by (91) with $\epsilon = 1$, $p = 0.5$, and $T = 3$. The images shown in Fig. 9 are what we judged to be the best that the respective anisotropic diffusion schemes can generate with respect to the diffusion time.

In the second experiment, the Cameraman image shown in Fig. 10 (top) is degraded to give the image shown in Fig. 10 (bottom) using Gaussian noise at SNR = 10 dB. We first employ the Perona and Malik diffusion (2) to process this degraded image and show two of the processed images in the top and middle of Fig. 11 (diffusion time $t = 64$ and 2048, respectively) which, as before, indicate that this diffusion scheme is incapable of dealing with noise. We then use the new scheme given by (91) with $\epsilon = 1$, $p = 0.5$, and $T =$

3. One of the processed images is shown in the bottom of Fig. 11 (diffusion time $t = 64$).

VIII. CONCLUSIONS

In this paper, we have provided a behavioral analysis of the anisotropic diffusion model of Perona and Malik. The main idea was to express the equation as coming from a certain optimization problem and find conditions for the existence of a unique global minimum (well-posed diffusion) and for the existence of infinitely many dense global minima (ill-posed diffusion). In addition, the smoothing and edge enhancement mechanism of anisotropic diffusion is illustrated through an eigenvalue decomposition of the diffusion equation. Moreover, we gave a natural geometric interpretation of this decomposition and found that the two terms involved were dual in a certain precise sense. As indicated above, we will be extending these results to the vector case (in particular, to color space) in the near future.

REFERENCES

[1] L. Alvarez, P.-L. Lions, and J.-M. Morel, "Image selective smoothing and edge detection by nonlinear diffusion II," *SIAM Numer. Anal.,* vol. 29, no. 3, pp. 845–866, June 1992.

[2] L. Alvarez, F. Guichard, P. L. Lions, and J. M. Morel, "Axiomatization et nouveaux operateurs de la morphologie mathematique," *C. R. Acad. Sci. Paris,* vol. 315, pp. 265–268, 1992.

[3] _____, "Axiomes et equations fondamentales du traitement d'images," *C. R. Acad. Sci. Paris,* vol. 315, pp. 135–138, 1992.

[4] S. Angenent, "Parabolic equations for curves on surfaces, I: Curves with p-integrable curvature," *Ann. Math.,* vol. 133, pp. 451–483, 1990.

[5] _____, "Parabolic equations for curves on surfaces, II: Intersections, blow-up, and generalized solutions," *Ann. Math.,* vol. 133, pp. 171–215, 1991.

[6] M. S. Bazaraa and C. M. Shetty, *Nonlinear Programming: Theory and Algorithms.* New York: Wiley, 1979.

[7] M. Bertero, T. A. Poggio, and V. Torre, "Ill-posed problems in early vision," *Proc. IEEE,* vol. 76, no. 8, pp. 869–889, Aug. 1988.

[8] F. Catte, P.-L. Lions, J.-M. Morel, and T. Coll, "Image selective smoothing and edge detection by nonlinear diffusion," *SIAM J. Num. Anal.,* vol. 29, no. 1, pp. 182–193, Feb. 1992.

[9] V. Caselles, F. Catte, T. Coll, and F. Dibos, "A geometric model for active contours in image processing," *AMS,* vol. 29, pp. 1–10, 1993.

[10] M. G. Crandall, H. Ishii, and P. L. Lions, "Users guide to viscosity solutions of second order partial linear differential equations," *Bull. Amer. Math. Soc.,* vol. 27, pp. 1–67, 1992.

[11] L. C. Evans, "Estimates for smooth absolutely minimizing Lipschitz extensions," *Electron. J. Differen. Equat.,* vol. 1, pp. 1–9, 1993.

[12] L. C. Evans and J. Spruck, "Motion of level sets by mean curvature, I," *J. Differen. Geom.,* vol. 33, pp. 635–681, 1991.

[13] L. Florack, "The syntactical structure of scalar images," Ph.D. dissertation, Univ. Utrecht, The Netherlands, Nov. 1993.

[14] M. Gage and R. S. Hamilton, "The heat equation shrinking convex plane curves," *J. Differen. Geom.,* vol. 23, pp. 285–314, 1986.

[15] M. Grayson, "The heat equation shrinks embedded plane curves to round points," *J. Differen. Geom.,* vol. 26, pp. 285–314, 1987.

[16] _____, "Shortening embedded curves," *Ann. Math.,* vol. 129, pp. 71–111, 1989.

[17] J. Hadamard, *Lectures on the Cauchy Problem in Linear Partial Differential Equations.* New Haven: Yale Univ. Press, 1923.

[18] K. Hollig and J. A. Nohel, "A diffusion equation with a nonmonotone constitutive function," in *Proc. Syst. Nonlinear Partial Differen. Equation,* J. Ball, Ed. Boston: D. Reidel, 1983, pp. 409–422.

[19] S. Kichenassamy, "The Perona–Malik paradox," Department of Mathematics, Tech. Rep., Univ. Minnesota, Minneapolis, MN, 1996.

[20] B. Kimia, A. Tannenbaum, and S. Zucker, "Toward a computational theory of shape: An overview," Tech. Rep. Cim-89-13, McGill Univ., Montreal, Canada, 1989.

[21] _____, "On the evolution of curves via a function of curvature I," *J. Math. Anal. App.,* vol. 163, pp. 438–458, 1992.

[22] R. J. LeVeque, *Numerical Method for Conservation Laws.* Basel, Switzerland: Birkhauser, 1992.

[23] F. Mokhatarian and A. Mackworth, "A theory of multiscale, curvature-based shape representation for planar curves," *IEEE Trans. Pattern Anal. Machine Intell.,* vol. 14, pp. 789–805, 1992.

[24] A. W. Naylor and G. R. Sell, *Linear Operator Theory in Engineering and Science.* New York: Springer-Verlag, 1982.

[25] M. Nitzberg and T. Shiota, "Nonlinear image filtering with edge and corner enhancement," *IEEE Trans. Pattern Anal. Machine Intell.,* vol. 14, no. 8, pp. 826–833, Aug. 1992.

[26] S. J. Osher and J. A. Sethian, "Fronts propagating with curvature dependent speed: Algorithms based on Hamilton–Jacobi formulations," *J. Computat. Phys.,* vol. 79, pp. 12–49, 1988.

[27] P. Perona and J. Malik, "Scale-space and edge detection using anisotropic diffusion," *IEEE Trans. Pattern Anal. Machine Intell.,* vol. 12, no. 7, pp. 629–639, July 1990.

[28] W. Rudin, *Real and Complex Analysis.* New York: McGraw-Hill, 1966.

[29] L. I. Rudin, S. Osher, and E. Fatemi, "Nonlinear total variation based noise removal algorithms," *Physica D 60,* pp. 259–268, 1992.

[30] G. Sapiro and A. Tannenbaum, "Affine invariant scale-space," *Int. J. Comput. Vision,* no. 11.1, pp. 25–44, 1993.

[31] J. A. Sethian, "An analysis of flame propagation," Ph.D. dissertation, Univ. Calif., Berkeley, June 1982.

[32] _____, "Curvature and the evolution of fronts," *Commun. Math. Phys.,* vol. 101, pp. 487–499, 1985.

[33] _____, "A review of recent numerical algorithms for hypersurfaces moving with curvature dependent speed," *J. Differen. Geom.,* vol. 31, pp. 131–161, 1989.

[34] P. Smith, *Convexity Methods in Variational Calculus.* Letchworth, England: Research Studies Press Ltd., 1985.

[35] R. T. Whitaker and G. Gerig, "Vector-valued diffusion," in *Geometry-Driven Diffusion in Computer Vision,* Bart ter Haar Romeny, Ed. Boston: Kluwer, 1994, pp. 93–134.

[36] R. T. Whitaker and S. M. Pizer, "A multi-scale approach to nonuniform diffusion," *CVGIP: Image Understanding,* vol. 57, no. 1, pp. 99–110, Jan. 1993.

[37] Y.-L. You, M. Kaveh, Wenyuan Xu, and A. Tannenbaum, "Analysis and design of anisotropic diffusion for image processing," in *Proc. IEEE Int. Conf. Image Processing,* vol. II, Austin, TX, Nov. 1994, pp. 497–501.
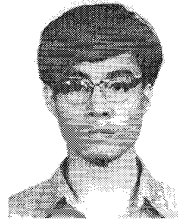
Yu-Li You received the B.S. and M.S. degrees in electronic engineering from Xidian University (Northwestern Telecommunication Engineering Institute), Xi'an, China, in 1985 and 1988, respectively, and the Ph.D. degree in electrical engineering from the University of Minnesota, Minneapolis, in 1995.

He has been a senior software engineer with Seagate Technology, Inc. since 1995. His current research interests include image and video compression, image enhancement, image restoration, image analysis, communications, and neural networks.

Dr. You received the 1990 Science and Technology Award from Guangdong Provincial Government of China.

Wenyuan Xu graduated from the Department of Mathematics, Nankai University, Tianjin, China, in 1963, and received the Ph.D. degree from the University of Minnesota, Minneapolis, in 1993.

From 1963 to 1979, he taught at Nankai University. From 1979 to 1990, he worked as a Research Assistant Professor, a Research Associate Professor, and a Research Professor, respectively, at the Institute of Systems Science, Academia Sinica, Beijing, China. From 1981 to 1983, and from 1986 to 1988, he was a Visiting Scholar and Visiting Professor, respectively, with the Department of Electrical Engineering, Polytechnic University, NY. From 1993 to 1995, he was a Visiting Professor with the Department of Electrical Engineering of the University of Minnesota. He is presently with the 3M company in Minnesota. His primary research interests are in signal processing, image processing, and statistical theory of communication.

Allen Tannenbaum was born in New York City in 1953. He received the Ph.D. in mathematics from Harvard University, Cambridge, MA, in 1976.

He has held faculty positions at the Weizmann Institute of Science, McGill University, University of Florida, ETH, Zurich, Switzerland, Technion–Israel Institute of Technology, and Ben-Gurion University of the Negev. He is presently Professor of Electrical Engineering at the University of Minnesota, Minneapolis. He has done research in robust control, systems theory, computer vision, image processing, robotics, semiconductor process control, operator theory, functional analysis, algebraic geometry, and invariant theory. Dr. Tannenbaum has authored or coauthored more than 170 research papers, and is the author or coauthor of three books: *Invariance and Systems Theory, Feedback Control Theory* (with J. Doyle and B. Francis), and *Robust Control of Infinite Dimensional Systems* (with C. Foias and H. Ozbay). He also edited a volume with B. Francis (in honor of George Zames) entitled *Feedback Control, Nonlinear Systems, and Complexity.*

Mostafa Kaveh (S'73–M'75–SM'83–F'88) received the B.S. and Ph.D. degrees in electrical engineering from Purdue University, West Lafayette, IN, in 1969 and 1974, respectively, and the M.S. degree from the University of California, Berkeley, in 1970. He has been at the University of Minnesota, Minneapolis, since 1975, where he is presently a Professor and Head of the Department of Electrical Engineering.

Dr. Kaveh is Vice President for Publications of the IEEE Signal Processing Society and was the General Chairman of ICASSP'93. He received a 1986 ASSP Senior (best paper) Award (with A. Barabell) and the 1988 ASSP Meritorious Service Award.